EUROPEAN ORGANIZATION FOR NUCLEAR RESEARCH

CERN-EP/2003-020
May 5, 2003

Measurement of Exclusive $\rho^0\rho^0$ Production in Two-Photon Collisions at High Q^2 at LEP

The L3 Collaboration

Abstract

Exclusive $\rho^0\rho^0$ production in two-photon collisions involving a single highly virtual photon is studied with data collected at LEP at centre-of-mass energies 89 GeV $< \sqrt{s} <$ 209 GeV with a total integrated luminosity of 854.7 pb^{-1}. The cross section of the process $\gamma\gamma^* \to \rho^0\rho^0$ is determined as a function of the photon virtuality, Q^2, and the two-photon centre-of-mass energy, $W_{\gamma\gamma}$, in the kinematic region: 1.2 GeV$^2 < Q^2 <$ 30 GeV^2 and 1.1 GeV $< W_{\gamma\gamma} <$ 3 GeV.

Submitted to *Phys. Lett. B*

1 Introduction

The exclusive production of ρ^0 meson pairs in two-photon collisions was studied by several experiments [1, 2]. A prominent feature of the reaction $\gamma\gamma \to \rho^0\rho^0$ is the broad cross section enhancement observed near threshold, the origin of which is still not well understood [3]. Most experiments studied $\rho^0\rho^0$ production by quasi-real photons, whereas only scarce data involving highly off-shell virtual photons are available [2]. The interest in exclusive production of hadron pairs in two-photon interactions at high momentum transfer was recently renewed since methods for calculating the cross section of such processes were developed in the framework of perturbative QCD [4]. In these models, the exclusive process is factorisable into a perturbative, calculable, short distance scattering $\gamma\gamma^* \to q\bar{q}$ or $\gamma\gamma^* \to gg$ and non-perturbative matrix elements describing the transition of the two partons into hadron pairs, which are called generalized distribution amplitudes.

This Letter presents results on the study of the two-photon reaction:

$$e^+e^- \to e^+e^-\gamma\gamma^* \to e^+e^-\rho^0\rho^0, \tag{1}$$

where one of the interacting virtual photons is quasi-real, γ, and the other one, γ^*, is highly virtual. The squared four-momentum, Q^2, of a virtual photon emitted by the incident beam electron[1)] is related to the beam energy, E_b, and to the energy and scattering angle of the outgoing electron, E_s and θ_s by:

$$Q^2 = 2E_bE_s(1 - \cos\theta_s). \tag{2}$$

A scattered electron detected ("tagged") by the forward electromagnetic calorimeter used to measure the luminosity corresponds to an off-shell photon with a large Q^2. The rate of such processes is considerably reduced as compared to production by quasi-real photons due to the sharp forward peaking of the angular distribution of the scattered electron.

The data used in this study correspond to an integrated luminosity of 854.7 pb^{-1} and were collected by the L3 detector [5] at LEP. Of this sample, 148.7 pb^{-1} were collected at e^+e^- centre-of-mass energies, $\sqrt{s}$, around the Z resonance (Z-pole), with average $\sqrt{s}$ of 91 GeV and 706.0 pb^{-1} at centre-of-mass energies in the range 161 GeV $\leq \sqrt{s} <$ 209 GeV (high energy), corresponding to an average $\sqrt{s}$ of 195 GeV. This Letter presents the production cross section as a function of Q^2 in the restricted kinematical regions

$$1.2 \text{ GeV}^2 < Q^2 < 8.5 \text{ GeV}^2 \quad (\text{Z} - \text{pole}) \tag{3}$$

and

$$8.8 \text{ GeV}^2 < Q^2 < 30 \text{ GeV}^2 \quad (\text{high energy}), \tag{4}$$

and the two-photon mass interval 1.1 GeV $< W_{\gamma\gamma} <$ 3 GeV. The data are compared to Vector Dominance models [6] and to a recent QCD model [7].

2 Event Selection

2.1 Exclusive four-track events

The reaction (1), contributing to the process

$$e^+e^- \to e^+e^-\pi^+\pi^-\pi^+\pi^-, \tag{5}$$

[1)] Throughout this Letter, the term "electron" denotes both electrons and positrons.

is identified by a scattered electron and four charged pions measured in the L3 detector. Tagged two-photon events are accepted by several independent triggers: two charged-particle triggers [8] and an energy trigger demanding a large energy deposition in the luminosity monitor in coincidence with at least one track [9]. The combined trigger efficiency, as determined from the data itself, is $(93.6 \pm 1.3)\%$ at the Z-pole and $(97.9 \pm 0.6)\%$ at high energy.

Single-tagged events are selected by requiring an electromagnetic cluster with energy greater then 80% of the beam energy reconstructed in the luminosity monitor, which covers the range 25 mrad $< \theta <$ 68 mrad of the electron scattering angle. At high energy the lower bound increases up to 31 mrad due to the installation of a mask to protect the detector from the beam halo.

Event candidates are required to have exactly four tracks, with zero total charge and with a polar angle, θ, relative to the beam direction, such that $|\cos\theta| \leq 0.94$. A track should come from the interaction vertex and have transverse momentum greater than 100 MeV. In addition, four-track events, incompatible with the pion mass hypothesis, are rejected using the energy loss information.

Events containing muons are removed from the sample. A search for secondary vertices is performed, and events with reconstructed short-lived neutral kaons are rejected. An event candidate is allowed to contain no more than one electromagnetic cluster, with an energy below 300 MeV and not exceeding 10% of the total energy of the four-pion system.

To ensure that an exclusive final state is detected, the momenta of the tagged electron and the four-pion system should be well balanced in the plane transverse to the beam direction. Thus the total transverse momentum squared, p_t^2, including the scattered electron, is required to be less than 0.2 GeV^2. This cut is also effectively a cut on the virtuality of the photon emitted by the untagged electron and thus ensures that the Q^2 variable, calculated from the measured parameters of the tagged electron using (2), corresponds to the photon with the highest virtuality.

2.2 Background estimation

The contribution to the selected sample due to e^+e^- annihilation is negligible. The background is mainly due to feed-down from tagged two-photon interactions producing a higher multiplicity final state, which is incompletely reconstructed. To estimate this effect two background-like data samples are selected. Firstly, we apply the same selection procedure discussed above releasing the charge-conservation requirement. Events of the types $\pi^+\pi^+\pi^+\pi^-$ and $\pi^+\pi^-\pi^-\pi^-$ are selected, in which at least two charged particles were undetected. Secondly, we select $\pi^+\pi^-\pi^+\pi^-\pi^0$ events, requiring the $\pi^+\pi^-\pi^+\pi^-$ subsystem to pass the four-pion selection discussed above without imposing the p_t^2 cut, and to contain in addition exactly two photons with effective mass in the range of $\pm$15 MeV around the π^0 mass. We require $p_t^2 < 0.2$ GeV^2 in order to select tagged exclusive $\pi^+\pi^-\pi^+\pi^-\pi^0$ events, and then consider only their $\pi^+\pi^-\pi^+\pi^-$ subsystem to represent the background contribution. We assume that a combination of these two data samples gives a good description of the background from partially reconstructed events. Their p_t^2 distributions, combined with the distribution of reconstructed Monte Carlo four-pion events, agree with the p_t^2 distribution observed in the data. These distributions are shown in Figure 1 for the restricted Q^2-ranges (3) and (4).

3 Data analysis

3.1 Selected Sample

In the region of four-pion mass $W_{\gamma\gamma} > 1$ GeV, 851 events are selected, 498 events at the Z-pole and 353 at high energy. The four-pion mass spectrum of the selected events is shown in Figure 2a.

The mass distributions of $\pi^+\pi^-$ combinations, shown in Figures 2b and 2c, exhibit a clear ρ^0 signal, while the mass distribution of $\pi^\pm\pi^\pm$ combinations, shown in Figure 2d, has no resonance structure. In Figure 2b, the clustering of entries in the region of the crossing of the ρ^0 mass-bands gives evidence for a contribution of $\rho^0\rho^0$ intermediate states.

The $\rho^0\rho^0$ production rate is determined as a function of Q^2 and $W_{\gamma\gamma}$. The resolution of the reconstructed variables Q^2 and $W_{\gamma\gamma}$ is better than 3% and thus the event migration between adjacent bins is negligible.

3.2 Monte Carlo Modelling

To estimate the number of $\rho^0\rho^0$ events in the selected four-pion data sample, we consider non-interfering contributions from three processes:

$$\begin{aligned} &\gamma\gamma^* \to \rho^0\rho^0; \\ &\gamma\gamma^* \to \rho^0\pi^+\pi^-; \\ &\gamma\gamma^* \to \pi^+\pi^-\pi^+\pi^-, \text{ non} - \text{resonant}. \end{aligned} \tag{6}$$

The data statistics is not sufficient to reach conclusions about contributions from subprocesses involving production of higher-mass resonances such as the $f_2(1270)$. Therefore in the present analysis we assume that the data is described by the processes (6) only. It was demonstrated that such a model provides a good description of exclusive four-pion production by quasi-real photons [1].

Monte Carlo samples of the process (6) are generated with the EGPC [10] program. About two million events of each process are produced for both the Z-pole and the high energy regions. The $W_{\gamma\gamma}$ and Q^2-dependence are those of the $\gamma\gamma$ luminosity function [11] and only isotropic production and phase space decays are included. These events are processed in the same way as the data, introducing specific detector inefficiencies for the different data taking periods.

For acceptance calculations, the Monte Carlo events are assigned a Q^2-dependent weight, evaluated using the GVDM [12] form-factor for both photons. Taking into account the detector acceptance and the efficiency of the selection procedure, the detection efficiency for each Q^2 and $W_{\gamma\gamma}$ bin is listed in Tables 1–3. It is in the range of $10\% - 25\%$, almost independent of the process. It slowly increases with Q^2 and slowly decreases with $W_{\gamma\gamma}$.

3.3 Fit Method

In order to determine the differential $\rho^0\rho^0$ production rate, a maximum likelihood fit to the data of the sum of the processes (6) is performed in intervals of Q^2 and $W_{\gamma\gamma}$. The set, Ω, of six two-pion masses, the four $\pi^+\pi^-$ combinations and the two $\pi^\pm\pi^\pm$ combinations, provides a complete description of a four-pion event in our model of isotropic production and decay discussed above. This choice of kinematic variables allows to fully exploit the information specific to each one of the processes (6) and to obtain their contributions to the observed four-pion yield. For each

data event, i, with measured variables Ω_i, we calculate the probabilities, $\mathrm{P}_j(\Omega_i)$, that the event resulted from the production mechanism j. The likelihood function is defined as:

$$\Lambda = \prod_i \sum_{j=1}^{3} \lambda_j \mathrm{P}_j(\Omega_i)\,, \qquad \sum_{j=1}^{3} \lambda_j = 1, \tag{7}$$

where λ_j is the fraction of the process j in the $\pi^+\pi^-\pi^+\pi^-$ sample for a given Q^2 or $W_{\gamma\gamma}$ bin and the product runs over all data events in that bin. The probabilities P_j are determined by the six-fold differential cross sections of the corresponding process, using Monte Carlo samples and a box method [13].

The fitting procedure is tested by applying it on various mixtures of Monte Carlo event samples from the processes (6), treated as data. The contribution of the $\rho^0\rho^0$ production process is always reproduced within statistical uncertainties, whereas, for small statistics test samples, large negative correlations, in the range of 60% – 75%, exist between the $\rho^0\pi^+\pi^-$ and $\pi^+\pi^-\pi^+\pi^-$ (non-resonant) fractions. Both contributions are, however, necessary to fit the data. Therefore, in the following, only the $\rho^0\rho^0$ content and the sum of the $\rho^0\pi^+\pi^-$ and $\pi^+\pi^-\pi^+\pi^-$ (non-resonant) contributions are considered.

To check the quality of the fit, the two-pion mass distributions of the data are compared with those of a mixture of Monte Carlo event samples from the processes (6), in the proportion determined by the fit. The data and Monte Carlo distributions are in good agreement over the whole Q^2 and $W_{\gamma\gamma}$ range; an example is shown in Figure 3.

As pointed out in Reference 14, the $\pi^+\pi^-$ system in the $\rho^0\pi^+\pi^-$ final state cannot have an isotropic angular distribution, since, in order to conserve C-parity, the angular momentum between the two pions has to be odd. We have verified that our results are insensitive to variations of the underlying angular distributions in the production model. In addition, a good agreement of the measured angular distributions of the data with those of the Monte Carlo is observed, as presented in Figure 4.

4 Results

4.1 Cross Sections

The cross sections, $\Delta\sigma_{\mathrm{ee}}$, of the process $\mathrm{e^+e^-} \to \mathrm{e^+e^-}\rho^0\rho^0$ are measured as a function of Q^2 and $W_{\gamma\gamma}$ and are listed in Tables 1–3 together with the efficiencies and background contamination. The statistical uncertainties, listed in the Tables, follow from the fit. The differential cross section $d\sigma_{\mathrm{ee}}/dQ^2$ of the process (1), derived from $\Delta\sigma_{\mathrm{ee}}$, is also listed in Table 1. When evaluating the differential cross section, a correction, based on the Q^2-dependence of the $\rho^0\rho^0$ Monte Carlo sample, is applied, such as to assign the cross section value to the centre of the corresponding Q^2-bin [15].

To evaluate the cross section $\sigma_{\gamma\gamma}$ of the process $\gamma\gamma^* \to \rho^0\rho^0$, the integral of the transverse photon luminosity function, L_{TT}, is computed for each Q^2 and $W_{\gamma\gamma}$ bin using the program GALUGA [16], which performs exact QED calculations. The cross section $\sigma_{\gamma\gamma}$ is derived from the measured cross section $\Delta\sigma_{\mathrm{ee}}$ using the relation $\Delta\sigma_{\mathrm{ee}} = L_{TT}\sigma_{\gamma\gamma}$. Thus $\sigma_{\gamma\gamma}$ represents an effective cross section containing contributions from both transverse (T) and longitudinal (L) photon polarizations:

$$\sigma_{\gamma\gamma}(W_{\gamma\gamma}, Q^2) = \sigma_{TT}(W_{\gamma\gamma}, Q^2) + \epsilon\sigma_{TL}(W_{\gamma\gamma}, Q^2)\,, \tag{8}$$

where σ_{TT} and σ_{TL} are the cross sections for collision of transverse-transverse and transverse-longitudinal photons. The ratio of longitudinal to transverse polarization of the virtual photon, ϵ, given, approximately, by the expression:

$$\epsilon \approx \frac{2E_s/E_b}{1+(E_s/E_b)^2}\,, \tag{9}$$

is greater than 0.98, for our data.

The cross section of the process $\gamma\gamma^* \to \rho^0\rho^0$ as a function of $W_{\gamma\gamma}$, listed in Table 2 and 3, is plotted in Figure 5 together with the sum of the cross sections of the processes $\gamma\gamma^* \to \rho^0\pi^+\pi^-$ and $\gamma\gamma^* \to \pi^+\pi^-\pi^+\pi^-$(non-resonant). The statistical uncertainties of the sum of these two cross sections take into account their correlations. The $\rho^0\rho^0$ cross section is dominated by a broad enhancement at threshold, already observed in the data at $Q^2 \approx 0$ [1] and at moderate Q^2 [2]. The two cross sections are listed in Table 1 and plotted in Figure 6a as a function of Q^2 .

4.2 Systematics

The uncertainty on this measurement is dominated by statistics. The uncertainty on the measured cross section due to the selection procedure, estimated by varying the cuts, is in the range $7\% - 20\%$, affecting more the higher Q^2 region. Different form-factor expressions used for reweighting the Monte Carlo events and the variation of the acceptance contribute to an overall shift in the range $2\% - 6\%$. The fitting procedure uncertainty mostly depends on the box size. It is estimated to be in the range $7\% - 18\%$ for the fits in Q^2 and in the range $8\% - 30\%$ for the fits in $W_{\gamma\gamma}$.

To estimate the uncertainties of the background correction, the background determination procedure is performed using only the $\pi^\pm\pi^\pm\pi^\pm\pi^\mp$ or only the $\pi^+\pi^-\pi^+\pi^-\pi^0$ samples. A contribution in the range $6\% - 11\%$ is obtained.

Collinear initial state radiation has little impact on the measurement since for 91% of the selected events the energy of the tagged electron exceeds 90% of the beam energy.

All the contributions are added in quadrature to obtain the systematic uncertainties quoted in Tables 1–3.

4.3 Fits to the Data

Figure 6b shows the result of a fit of the differential cross section $d\sigma_{\rm ee}/dQ^2$ to a form [17] expected from QCD-based calculations [7]:

$$d\sigma_{\rm ee}/dQ^2 \sim \frac{1}{Q^n(Q^2+ < W_{\gamma\gamma} >^2)^2}\,. \tag{10}$$

The fit is performed using the central value of the mass spectrum $< W_{\gamma\gamma} >= 1.94$ GeV. It provides a good description of the Q^2-dependence of the data with an exponent $n = 2.4 \pm 0.3$, to be compared with the expected value $n = 2$. Only statistical uncertainties are considered. A common fit of the data taken at the Z-pole and at high energy is justified by the almost constant values of the photon polarization parameter ϵ, which determines the energy dependence of the cross section.

In Figure 6a the data are fitted with two different form-factor parametrisations, leaving the normalization as a free parameter. A form suggested in Reference 6, based on the generalized

vector dominance model (GVDM) [12], provides a good description of the Q^2-dependence of the data whereas a steeper decrease is expected for a simple ρ-pole form-factor.

Acknowledgements

We thank M. Diehl and O. Teryaev for very useful discussions.

References

[1] TASSO Coll., R. Brandelik *et al.*, Phys. Lett. B **97** (1980) 448; M. Althoff *et al.*, Z. Phys. C **16** (1982) 13.
MARK II Coll., D.L. Burke *et al.*, Phys. Lett. B **103** (1981) 153.
CELLO Coll., H.-J. Behrend *et al.*, Z. Phys. C **21** (1984) 205.
ARGUS Coll., H. Albrecht *et al.*, Z. Phys. C **50** (1991) 1.

[2] PLUTO Coll., Ch. Berger *et al.*, Z. Phys. C **38** (1988) 521.
TPC/Two-Gamma Coll., H. Aihara *et al.*, Phys. Rev. D **37** (1988) 28.
TASSO Coll., W. Braunschweig *et al.*, Z. Phys. C **41** (1988) 353.

[3] N.N. Achasov *et al.*, Phys. Lett. B **108** (1982) 134; Z. Phys. C **16** (1982) 55; Phys. Lett. B **203** (1988) 309; G. Alexander *et al.*, Phys. Rev. D **26** (1982) 1198; Z. Phys. C **30** (1986) 65; B.A. Li and K.F. Liu, Phys. Lett. B **118** (1982) 435; Phys. Lett. B **124** (1983) 550; Phys. Rev. D **30** (1984) 613; Phys. Rev. Lett. **58** (1987) 2288; S.J. Brodsky, G. Köpp and P.M. Zerwas, Phys. Rev. Lett. **58** (1987) 443.

[4] M. Diehl, T. Gousset, B. Pire and O. Teryaev, Phys. Rev. Lett. **81** (1998) 1782.
A. Freund, Phys. Rev. D **61** (2000) 074010.
N. Kivel, L. Mankiewicz and M.V. Polyakov, Phys. Lett. B **467** (1999) 263.

[5] L3 Coll., B. Adeva *et al.*, Nucl. Instr. Meth. A **289** (1) (990) 35;
M. Acciarri *et al.*, Nucl. Instr. Meth. A **351** (1) (994) 300;
M. Chemarin *et al.*, Nucl. Instr. Meth. A **349** (1) (994) 345;
A. Adam *et al.*, Nucl. Instr. Meth. A **383** (1) (996) 342.

[6] I.F. Ginzburg and V.G. Serbo, Phys. Lett. B **109** (1982) 231.

[7] M. Diehl, T. Gousset and B. Pire. Phys. Rev. D **62** (2000) 073014.

[8] P. Béné *et al.*, Nucl. Instr. Meth. A **306** (1991) 150;
D. Haas *et al.*, Nucl. Instr. Meth. A **420** (1991) 101.

[9] R. Bizzarri *et al.*, Nucl. Instr. Meth. A **283** (1989) 799.

[10] F.L. Linde, PhD thesis, Rijksuniversiteit Leiden (1988).

[11] V.M. Budnev *et al.*, Phys. Rep. C **15** (1975) 181.

[12] J.J. Sakurai and D. Schildknecht, Phys. Lett. B **40** (1972) 121.

[13] D.M. Schmidt, R.J. Morrison and M.S. Witherell, Nucl. Instr. Meth. A **328** (1993) 547.

[14] N.N Achasov, S.A. Devyanin and G.N. Shestakov, Z. Phys. C **27** (1985) 99.

[15] G.D. Lafferty and T.R. Wyatt Nucl. Instr. Meth. A **355** (1995) 541.

[16] G.A. Schuler, Comput. Phys. Commun. **108** (1998) 279.

[17] M. Diehl private communication.

The L3 Collaboration:

P.Achard,[20] O.Adriani,[17] M.Aguilar-Benitez,[24] J.Alcaraz,[24] G.Alemanni,[22] J.Allaby,[18] A.Aloisio,[28] M.G.Alviggi,[28] H.Anderhub,[46] V.P.Andreev,[6,33] F.Anselmo,[8] A.Arefiev,[27] T.Azemoon,[3] T.Aziz,[9] P.Bagnaia,[38] A.Bajo,[24] G.Baksay,[25] L.Baksay,[25] S.V.Baldew,[2] S.Banerjee,[9] Sw.Banerjee,[4] A.Barczyk,[46,44] R.Barillère,[18] P.Bartalini,[22] M.Basile,[8] N.Batalova,[43] R.Battiston,[32] A.Bay,[22] F.Becattini,[17] U.Becker,[13] F.Behner,[46] L.Bellucci,[17] R.Berbeco,[3] J.Berdugo,[24] P.Berges,[13] B.Bertucci,[32] B.L.Betev,[46] M.Biasini,[32] M.Biglietti,[28] A.Biland,[46] J.J.Blaising,[4] S.C.Blyth,[34] G.J.Bobbink,[2] A.Böhm,[1] L.Boldizsar,[12] B.Borgia,[38] S.Bottai,[17] D.Bourilkov,[46] M.Bourquin,[20] S.Braccini,[20] J.G.Branson,[40] F.Brochu,[4] J.D.Burger,[13] W.J.Burger,[32] X.D.Cai,[13] M.Capell,[13] G.Cara Romeo,[8] G.Carlino,[28] A.Cartacci,[17] J.Casaus,[24] F.Cavallari,[38] N.Cavallo,[35] C.Cecchi,[32] M.Cerrada,[24] M.Chamizo,[20] Y.H.Chang,[48] M.Chemarin,[23] A.Chen,[48] G.Chen,[7] G.M.Chen,[7] H.F.Chen,[21] H.S.Chen,[7] G.Chiefari,[28] L.Cifarelli,[39] F.Cindolo,[8] I.Clare,[13] R.Clare,[37] G.Coignet,[4] N.Colino,[24] S.Costantini,[38] B.de la Cruz,[24] S.Cucciarelli,[32] J.A.van Dalen,[30] R.de Asmundis,[28] P.Déglon,[20] J.Debreczeni,[12] A.Degré,[4] K.Dehmelt,[25] K.Deiters,[44] D.della Volpe,[28] E.Delmeire,[20] P.Denes,[36] F.DeNotaristefani,[38] A.De Salvo,[46] M.Diemoz,[38] M.Dierckxsens,[2] C.Dionisi,[38] M.Dittmar,[46] A.Doria,[28] M.T.Dova,[10,♯] D.Duchesneau,[4] M.Duda,[1] B.Echenard,[20] A.Eline,[18] A.El Hage,[1] H.El Mamouni,[23] A.Engler,[34] F.J.Eppling,[13] P.Extermann,[20] M.A.Falagan,[24] S.Falciano,[38] A.Favara,[31] J.Fay,[23] O.Fedin,[33] M.Felcini,[46] T.Ferguson,[34] H.Fesefeldt,[1] E.Fiandrini,[32] J.H.Field,[20] F.Filthaut,[30] P.H.Fisher,[13] W.Fisher,[36] I.Fisk,[40] G.Forconi,[13] K.Freudenreich,[46] C.Furetta,[26] Yu.Galaktionov,[27,13] S.N.Ganguli,[9] P.Garcia-Abia,[24] M.Gataullin,[31] S.Gentile,[38] S.Giagu,[38] Z.F.Gong,[21] G.Grenier,[23] O.Grimm,[46] M.W.Gruenewald,[16] M.Guida,[39] R.van Gulik,[2] V.K.Gupta,[36] A.Gurtu,[9] L.J.Gutay,[43] D.Haas,[5] D.Hatzifotiadou,[8] T.Hebbeker,[1] A.Hervé,[18] J.Hirschfelder,[34] H.Hofer,[46] M.Hohlmann,[25] G.Holzner,[46] S.R.Hou,[48] Y.Hu,[30] B.N.Jin,[7] L.W.Jones,[3] P.de Jong,[2] I.Josa-Mutuberría,[24] D.Käfer,[1] M.Kaur,[14] M.N.Kienzle-Focacci,[20] J.K.Kim,[42] J.Kirkby,[18] W.Kittel,[30] A.Klimentov,[13,27] A.C.König,[30] M.Kopal,[43] V.Koutsenko,[13,27] M.Kräber,[46] R.W.Kraemer,[34] A.Krüger,[45] A.Kunin,[13] P.Ladron de Guevara,[24] I.Laktineh,[23] G.Landi,[17] M.Lebeau,[18] A.Lebedev,[13] P.Lebrun,[23] P.Lecomte,[46] P.Lecoq,[18] P.Le Coultre,[46] J.M.Le Goff,[18] R.Leiste,[45] M.Levtchenko,[26] P.Levtchenko,[33] C.Li,[21] S.Likhoded,[45] C.H.Lin,[48] W.T.Lin,[48] F.L.Linde,[2] L.Lista,[28] Z.A.Liu,[7] W.Lohmann,[45] E.Longo,[38] Y.S.Lu,[7] C.Luci,[38] L.Luminari,[38] W.Lustermann,[46] W.G.Ma,[21] L.Malgeri,[20] A.Malinin,[27] C.Maña,[24] J.Mans,[36] J.P.Martin,[23] F.Marzano,[38] K.Mazumdar,[9] R.R.McNeil,[6] S.Mele,[18,28] L.Merola,[28] M.Meschini,[17] W.J.Metzger,[30] A.Mihul,[11] H.Milcent,[18] G.Mirabelli,[38] J.Mnich,[1] G.B.Mohanty,[9] G.S.Muanza,[23] A.J.M.Muijs,[2] B.Musicar,[40] M.Musy,[38] S.Nagy,[15] S.Natale,[20] M.Napolitano,[28] F.Nessi-Tedaldi,[46] H.Newman,[31] A.Nisati,[38] T.Novak,[30] H.Nowak,[45] R.Ofierzynski,[46] G.Organtini,[38] I.Pal,[43]C.Palomares,[24] P.Paolucci,[28] R.Paramatti,[38] G.Passaleva,[17] S.Patricelli,[28] T.Paul,[10] M.Pauluzzi,[32] C.Paus,[13] F.Pauss,[46] M.Pedace,[38] S.Pensotti,[26] D.Perret-Gallix,[4] B.Petersen,[30] D.Piccolo,[28] F.Pierella,[8] M.Pioppi,[32] P.A.Piroué,[36] E.Pistolesi,[26] V.Plyaskin,[27] M.Pohl,[20] V.Pojidaev,[17] J.Pothier,[18] D.Prokofiev,[33] J.Quartieri,[39] G.Rahal-Callot,[46] M.A.Rahaman,[9] P.Raics,[15] N.Raja,[9] R.Ramelli,[46] P.G.Rancoita,[26] R.Ranieri,[17] A.Raspereza,[45] P.Razis,[29]D.Ren,[46] M.Rescigno,[38] S.Reucroft,[10] S.Riemann,[45] K.Riles,[3] B.P.Roe,[3] L.Romero,[24] A.Rosca,[45] S.Rosier-Lees,[4] S.Roth,[1] C.Rosenbleck,[1] J.A.Rubio,[18] G.Ruggiero,[17] H.Rykaczewski,[46] A.Sakharov,[46] S.Saremi,[6] S.Sarkar,[38] J.Salicio,[18] E.Sanchez,[24] C.Schäfer,[18] V.Schegelsky,[33] H.Schopper,[47] D.J.Schotanus,[30] C.Sciacca,[28] L.Servoli,[32] S.Shevchenko,[31] N.Shivarov,[41] V.Shoutko,[13] E.Shumilov,[27] A.Shvorob,[31] D.Son,[42] C.Souga,[23] P.Spillantini,[17] M.Steuer,[13] D.P.Stickland,[36] B.Stoyanov,[41] A.Straessner,[18] K.Sudhakar,[9] G.Sultanov,[41] L.Z.Sun,[21] S.Sushkov,[1] H.Suter,[46] J.D.Swain,[10] Z.Szillasi,[25,¶] X.W.Tang,[7] P.Tarjan,[15] L.Tauscher,[5] L.Taylor,[10] B.Tellili,[23] D.Teyssier,[23] C.Timmermans,[30] Samuel C.C.Ting,[13] S.M.Ting,[13] S.C.Tonwar,[9] J.Tóth,[12] C.Tully,[36] K.L.Tung,[7] J.Ulbricht,[46] E.Valente,[38] R.T.Van de Walle,[30] R.Vasquez,[43] V.Veszpremi,[25] G.Vesztergombi,[12] I.Vetlitsky,[27] D.Vicinanza,[39] G.Viertel,[46] S.Villa,[37] M.Vivargent,[4] S.Vlachos,[5] I.Vodopianov,[25] H.Vogel,[34] H.Vogt,[45] I.Vorobiev,[34,27] A.A.Vorobyov,[33] M.Wadhwa,[5] Q.Wang,[30] X.L.Wang,[21] Z.M.Wang,[21] M.Weber,[1] P.Wienemann,[1] H.Wilkens,[30] S.Wynhoff,[36] L.Xia,[31] Z.Z.Xu,[21] J.Yamamoto,[3] B.Z.Yang,[21] C.G.Yang,[7] H.J.Yang,[3] M.Yang,[7] S.C.Yeh,[49] An.Zalite,[33] Yu.Zalite,[33] Z.P.Zhang,[21] J.Zhao,[21] G.Y.Zhu,[7] R.Y.Zhu,[31] H.L.Zhuang,[7] A.Zichichi,[8,18,19] B.Zimmermann,[46] M.Zöller.[1]

1 III. Physikalisches Institut, RWTH, D-52056 Aachen, Germany[§]
2 National Institute for High Energy Physics, NIKHEF, and University of Amsterdam, NL-1009 DB Amsterdam, The Netherlands
3 University of Michigan, Ann Arbor, MI 48109, USA
4 Laboratoire d'Annecy-le-Vieux de Physique des Particules, LAPP,IN2P3-CNRS, BP 110, F-74941 Annecy-le-Vieux CEDEX, France
5 Institute of Physics, University of Basel, CH-4056 Basel, Switzerland
6 Louisiana State University, Baton Rouge, LA 70803, USA
7 Institute of High Energy Physics, IHEP, 100039 Beijing, China[△]
8 University of Bologna and INFN-Sezione di Bologna, I-40126 Bologna, Italy
9 Tata Institute of Fundamental Research, Mumbai (Bombay) 400 005, India
10 Northeastern University, Boston, MA 02115, USA
11 Institute of Atomic Physics and University of Bucharest, R-76900 Bucharest, Romania
12 Central Research Institute for Physics of the Hungarian Academy of Sciences, H-1525 Budapest 114, Hungary[‡]
13 Massachusetts Institute of Technology, Cambridge, MA 02139, USA
14 Panjab University, Chandigarh 160 014, India.
15 KLTE-ATOMKI, H-4010 Debrecen, Hungary[¶]
16 Department of Experimental Physics, University College Dublin, Belfield, Dublin 4, Ireland
17 INFN Sezione di Firenze and University of Florence, I-50125 Florence, Italy
18 European Laboratory for Particle Physics, CERN, CH-1211 Geneva 23, Switzerland
19 World Laboratory, FBLJA Project, CH-1211 Geneva 23, Switzerland
20 University of Geneva, CH-1211 Geneva 4, Switzerland
21 Chinese University of Science and Technology, USTC, Hefei, Anhui 230 029, China[△]
22 University of Lausanne, CH-1015 Lausanne, Switzerland
23 Institut de Physique Nucléaire de Lyon, IN2P3-CNRS,Université Claude Bernard, F-69622 Villeurbanne, France
24 Centro de Investigaciones Energéticas, Medioambientales y Tecnológicas, CIEMAT, E-28040 Madrid, Spain[♭]
25 Florida Institute of Technology, Melbourne, FL 32901, USA
26 INFN-Sezione di Milano, I-20133 Milan, Italy
27 Institute of Theoretical and Experimental Physics, ITEP, Moscow, Russia
28 INFN-Sezione di Napoli and University of Naples, I-80125 Naples, Italy
29 Department of Physics, University of Cyprus, Nicosia, Cyprus
30 University of Nijmegen and NIKHEF, NL-6525 ED Nijmegen, The Netherlands
31 California Institute of Technology, Pasadena, CA 91125, USA
32 INFN-Sezione di Perugia and Università Degli Studi di Perugia, I-06100 Perugia, Italy
33 Nuclear Physics Institute, St. Petersburg, Russia
34 Carnegie Mellon University, Pittsburgh, PA 15213, USA
35 INFN-Sezione di Napoli and University of Potenza, I-85100 Potenza, Italy
36 Princeton University, Princeton, NJ 08544, USA
37 University of Californa, Riverside, CA 92521, USA
38 INFN-Sezione di Roma and University of Rome, "La Sapienza", I-00185 Rome, Italy
39 University and INFN, Salerno, I-84100 Salerno, Italy
40 University of California, San Diego, CA 92093, USA
41 Bulgarian Academy of Sciences, Central Lab. of Mechatronics and Instrumentation, BU-1113 Sofia, Bulgaria
42 The Center for High Energy Physics, Kyungpook National University, 702-701 Taegu, Republic of Korea
43 Purdue University, West Lafayette, IN 47907, USA
44 Paul Scherrer Institut, PSI, CH-5232 Villigen, Switzerland
45 DESY, D-15738 Zeuthen, Germany
46 Eidgenössische Technische Hochschule, ETH Zürich, CH-8093 Zürich, Switzerland
47 University of Hamburg, D-22761 Hamburg, Germany
48 National Central University, Chung-Li, Taiwan, China
49 Department of Physics, National Tsing Hua University, Taiwan, China
§ Supported by the German Bundesministerium für Bildung, Wissenschaft, Forschung und Technologie
‡ Supported by the Hungarian OTKA fund under contract numbers T019181, F023259 and T037350.
¶ Also supported by the Hungarian OTKA fund under contract number T026178.
♭ Supported also by the Comisión Interministerial de Ciencia y Tecnología.
♯ Also supported by CONICET and Universidad Nacional de La Plata, CC 67, 1900 La Plata, Argentina.
△ Supported by the National Natural Science Foundation of China.

Q^2-range [GeV]	ε [%]	Bg [%]	$\Delta\sigma_{ee}$ [pb] $\rho^0\rho^0$	$d\,\sigma_{ee}/d\,Q^2$ [pb / GeV^2] $\rho^0\rho^0$	$\sigma_{\gamma\gamma}$ [nb] $\rho^0\rho^0$	$d\,\sigma_{ee}/d\,Q^2$ [pb / GeV^2] $\rho^0\pi^+\pi^- + \pi^+\pi^-\pi^+\pi^-$
1.2 – 1.7	9	31	$2.30 \pm 0.66 \pm 0.28$	$4.41 \pm 1.26 \pm 0.53$	$3.13 \pm 0.89 \pm 0.38$	$6.77 \pm 1.35 \pm 0.87$
1.7 – 2.5	12	27	$1.76 \pm 0.59 \pm 0.26$	$2.09 \pm 0.70 \pm 0.31$	$2.44 \pm 0.81 \pm 0.37$	$3.82 \pm 0.76 \pm 0.49$
2.5 – 3.5	14	21	$1.36 \pm 0.40 \pm 0.25$	$1.32 \pm 0.39 \pm 0.24$	$2.51 \pm 0.74 \pm 0.45$	$1.74 \pm 0.41 \pm 0.22$
3.5 – 5.5	15	16	$1.02 \pm 0.41 \pm 0.17$	$0.47 \pm 0.19 \pm 0.080$	$1.68 \pm 0.68 \pm 0.29$	$0.97 \pm 0.21 \pm 0.16$
5.5 – 8.5	18	6	$0.53 \pm 0.23 \pm 0.10$	$0.16 \pm 0.070 \pm 0.030$	$1.15 \pm 0.50 \pm 0.22$	$0.33 \pm 0.083 \pm 0.046$
8.8 – 13.0	16	11	$0.25 \pm 0.094 \pm 0.038$	$0.056 \pm 0.021 \pm 0.0085$	$0.58 \pm 0.21 \pm 0.09$	$0.17 \pm 0.025 \pm 0.019$
13.0 – 18.0	21	23	$0.080 \pm 0.042 \pm 0.022$	$0.015 \pm 0.0079 \pm 0.0041$	$0.27 \pm 0.14 \pm 0.07$	$0.044 \pm 0.0096 \pm 0.0065$
18.0 – 30.0	22	23	$0.075 \pm 0.047 \pm 0.022$	$0.0055 \pm 0.0035 \pm 0.0017$	$0.21 \pm 0.13 \pm 0.06$	$0.013 \pm 0.0040 \pm 0.0027$

Table 1: Detection efficiencies, ε, background fractions, Bg, and measured production cross sections as a function of Q^2 for 1.1 GeV $< W_{\gamma\gamma} <$ 3 GeV for Z-pole and high energy data. The values of the differential cross sections are corrected to the centre of each bin.

$W_{\gamma\gamma}$-range [GeV]	ε [%]	Bg [%]	$\Delta\sigma_{ee}$ [pb] $\rho^0\rho^0$	$\sigma_{\gamma\gamma}$ [nb] $\rho^0\rho^0$	$\sigma_{\gamma\gamma}$ [nb] $\rho^0\pi^+\pi^- + \pi^+\pi^-\pi^+\pi^-$
1.1 – 1.3	11	18	$0.56 \pm 0.31 \pm 0.14$	$1.42 \pm 0.79 \pm 0.36$	$2.24 \pm 0.88 \pm 0.41$
1.3 – 1.6	11	26	$1.64 \pm 0.49 \pm 0.28$	$2.91 \pm 0.87 \pm 0.50$	$3.75 \pm 0.92 \pm 0.56$
1.6 – 1.8	12	25	$1.53 \pm 0.47 \pm 0.26$	$4.32 \pm 1.34 \pm 0.73$	$4.41 \pm 1.35 \pm 0.79$
1.8 – 2.1	13	23	$1.54 \pm 0.60 \pm 0.35$	$3.10 \pm 1.20 \pm 0.71$	$5.87 \pm 1.31 \pm 0.88$
2.1 – 2.4	13	22	$0.80 \pm 0.39 \pm 0.20$	$1.75 \pm 0.86 \pm 0.44$	$5.72 \pm 1.06 \pm 0.81$
2.4 – 3.0	13	20	$0.64 \pm 0.30 \pm 0.13$	$0.79 \pm 0.37 \pm 0.16$	$3.22 \pm 0.52 \pm 0.39$
3.0 – 4.0	14	15	$0.09 \pm 0.12 \pm 0.07$	$0.08 \pm 0.11 \pm 0.06$	$1.23 \pm 0.24 \pm 0.17$

Table 2: Detection efficiencies, ε, background fractions, Bg, and measured production cross sections as a function of $W_{\gamma\gamma}$, for 1.2 GeV^2 $< Q^2 <$ 8.5 GeV^2, for the Z-pole data. The cross sections of the reaction $e^+e^- \to e^+e^-\rho^0\rho^0$, $\gamma\gamma^* \to \rho^0\rho^0$ and of the sum of the processes $\gamma\gamma^* \to \rho^0\pi^+\pi^-$ and $\gamma\gamma^* \to \pi^+\pi^-\pi^+\pi^-$(non-resonant) are also given. The first uncertainties are statistical, the second systematic.

$W_{\gamma\gamma}$-range [GeV]	ε [%]	Bg [%]	$\Delta\sigma_{ee}$ [pb] $\rho^0\rho^0$	$\sigma_{\gamma\gamma}$ [nb] $\rho^0\rho^0$	$\sigma_{\gamma\gamma}$ [nb] $\rho^0\pi^+\pi^- + \pi^+\pi^-\pi^+\pi^-$
1.1 – 1.3	22	19	$0.041 \pm 0.032 \pm 0.017$	$0.34 \pm 0.26 \pm 0.14$	$0.83 \pm 0.32 \pm 0.27$
1.3 – 2.0	19	23	$0.184 \pm 0.073 \pm 0.046$	$0.46 \pm 0.18 \pm 0.11$	$1.08 \pm 0.21 \pm 0.15$
2.0 – 3.0	17	9	$0.175 \pm 0.077 \pm 0.053$	$0.31 \pm 0.14 \pm 0.09$	$1.17 \pm 0.18 \pm 0.16$
3.0 – 4.0	16	9	$0.012 \pm 0.022 \pm 0.009$	$0.02 \pm 0.04 \pm 0.02$	$0.67 \pm 0.11 \pm 0.09$

Table 3: Detection efficiency, ε, background fractions, Bg, and measured production cross sections as a function of $W_{\gamma\gamma}$, for 8.8 GeV^2 $< Q^2 <$ 30 GeV^2, for the high energy data. The cross section of the reaction $e^+e^- \to e^+e^-\rho^0\rho^0$, $\gamma\gamma^* \to \rho^0\rho^0$ and of the sum of the processes $\gamma\gamma^* \to \rho^0\pi^+\pi^-$ and $\gamma\gamma^* \to \pi^+\pi^-\pi^+\pi^-$(non-resonant) are also given. The first uncertainties are statistical, the second systematic.

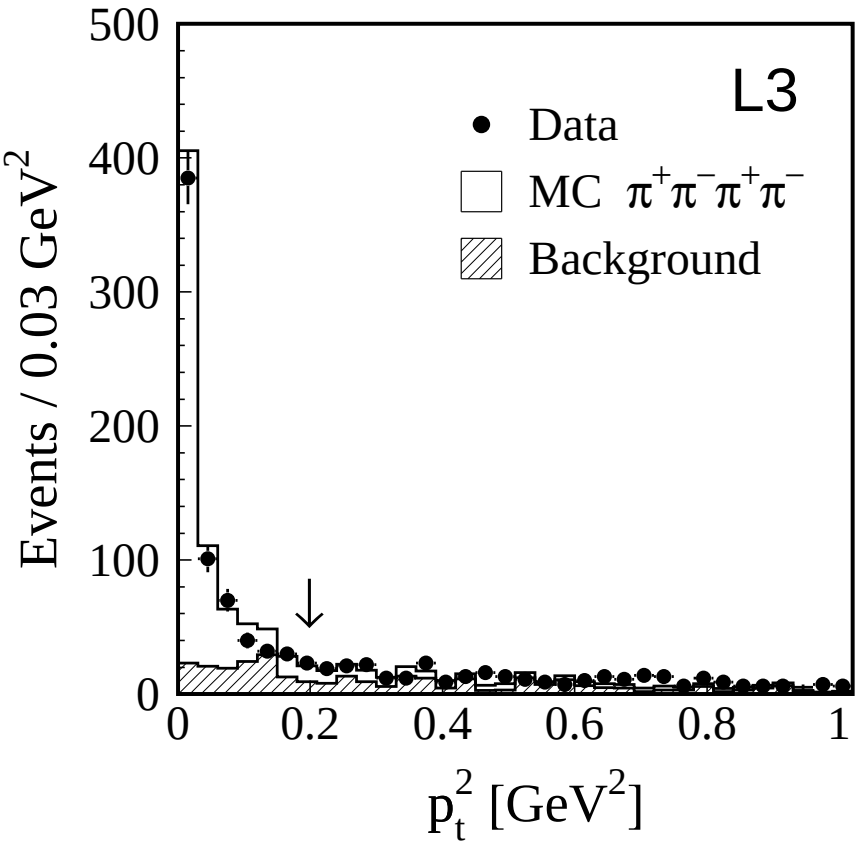

Figure 1: The p_t^2 distribution of the selected $\pi^+\pi^-\pi^+\pi^-$ data (points) in comparison with Monte Carlo distributions of four-pion events (open histogram) and the background estimated from the data (hatched histogram). The arrow indicates the selection cut on p_t^2.

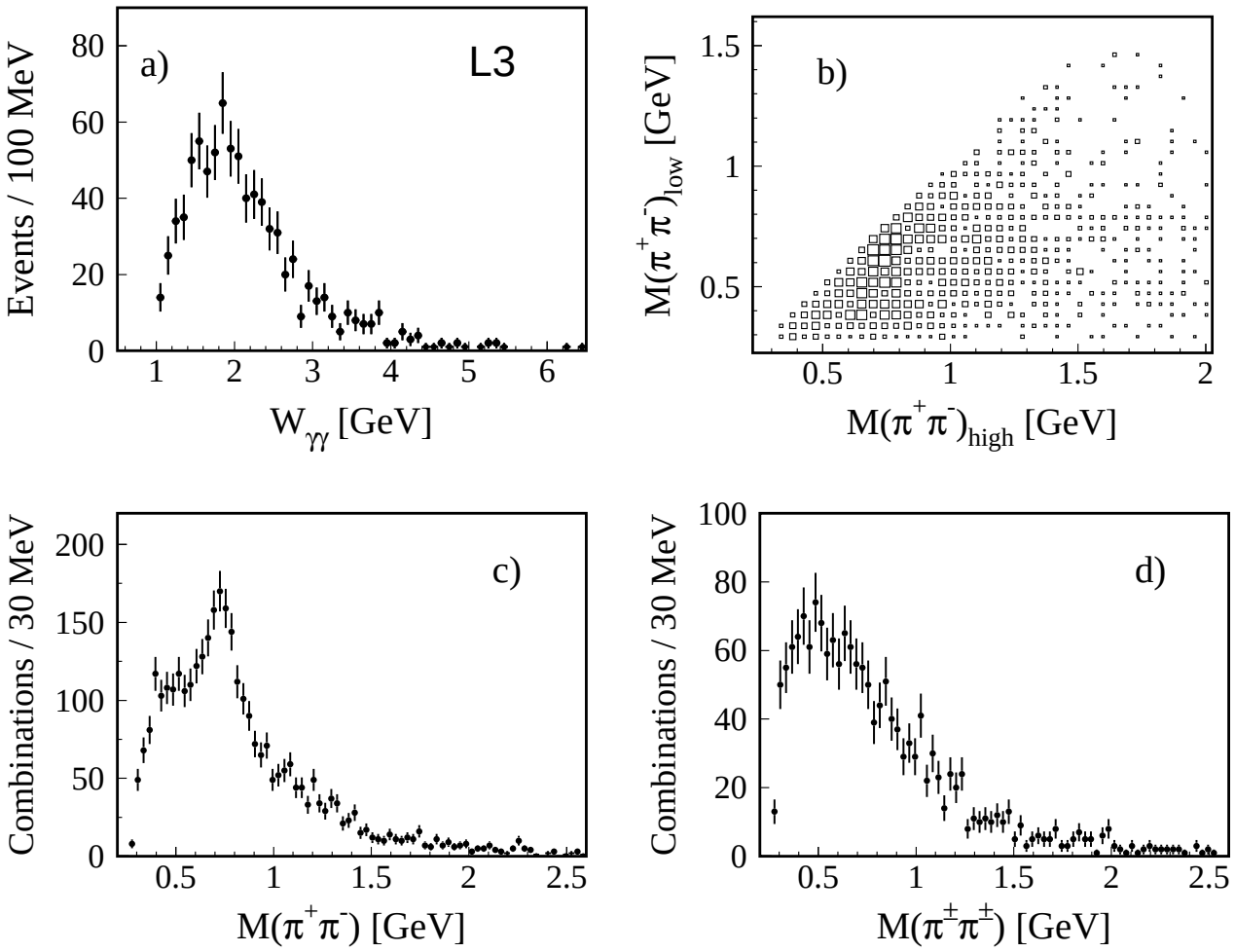

Figure 2: Effective mass distributions for the selected events: (a) Mass of the four-pion system, $W_{\gamma\gamma}$. (b) Correlation between the masses of two $\pi^+\pi^-$ pairs (two entries per event). The higher mass of each pair is plotted on the horizontal axis. (c) Mass of the $\pi^+\pi^-$ combinations (four entries per event). (d) Mass of the $\pi^\pm\pi^\pm$ combinations (two entries per event).

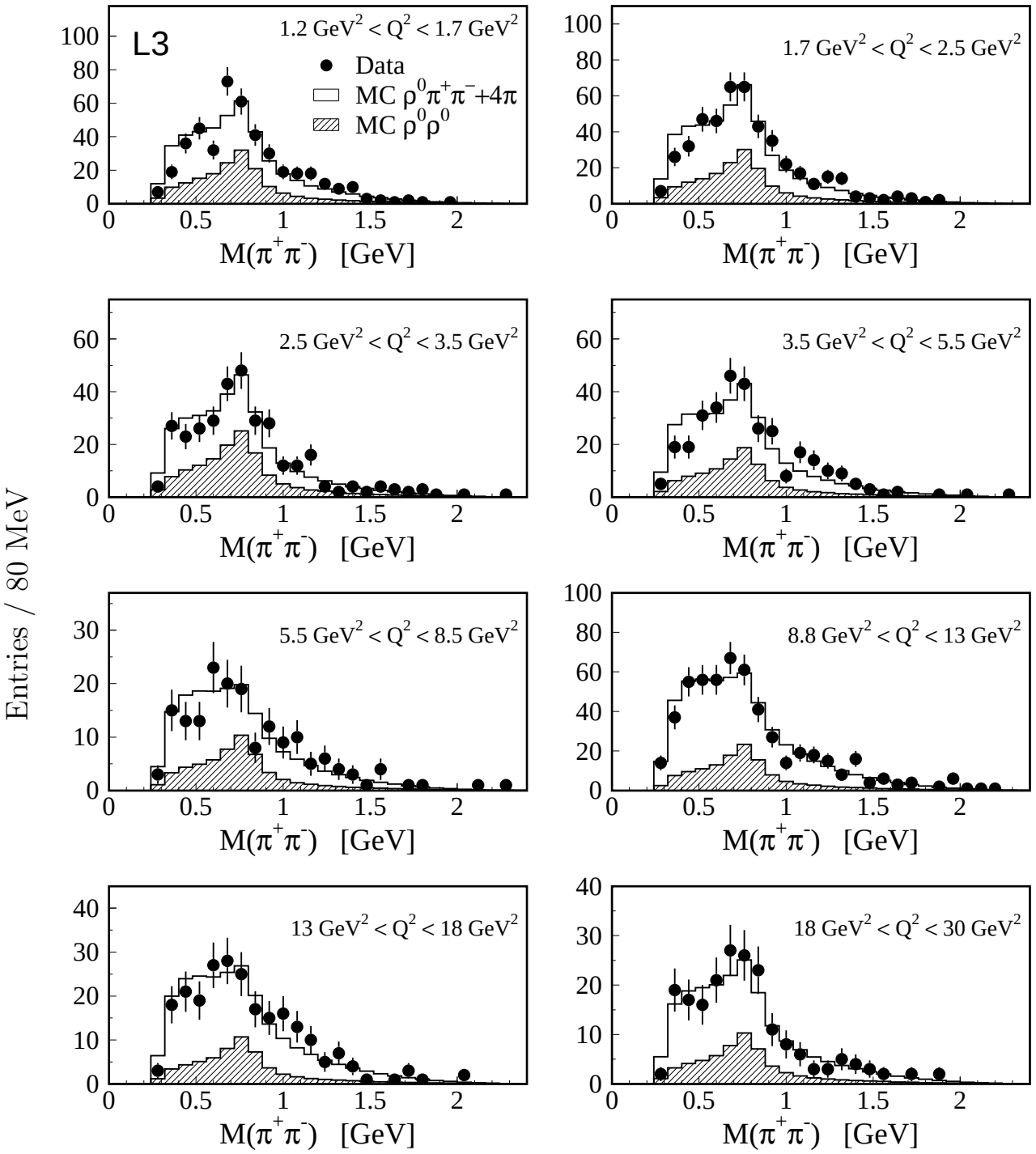

Figure 3: Mass distributions of $\pi^+\pi^-$ combinations (four entries per event) for events with 1.1 GeV $< W_{\gamma\gamma} <$ 3 GeV in the fitted Q^2 intervals. The points represent the data, the hatched area the $\rho^0\rho^0$ component, and the open area the sum of the $\rho^0\pi^+\pi^-$ and $\pi^+\pi^-\pi^+\pi^-$ (non-resonant) components. The fraction of the different components are determined by the fit and the total normalisation is to the number of the events.

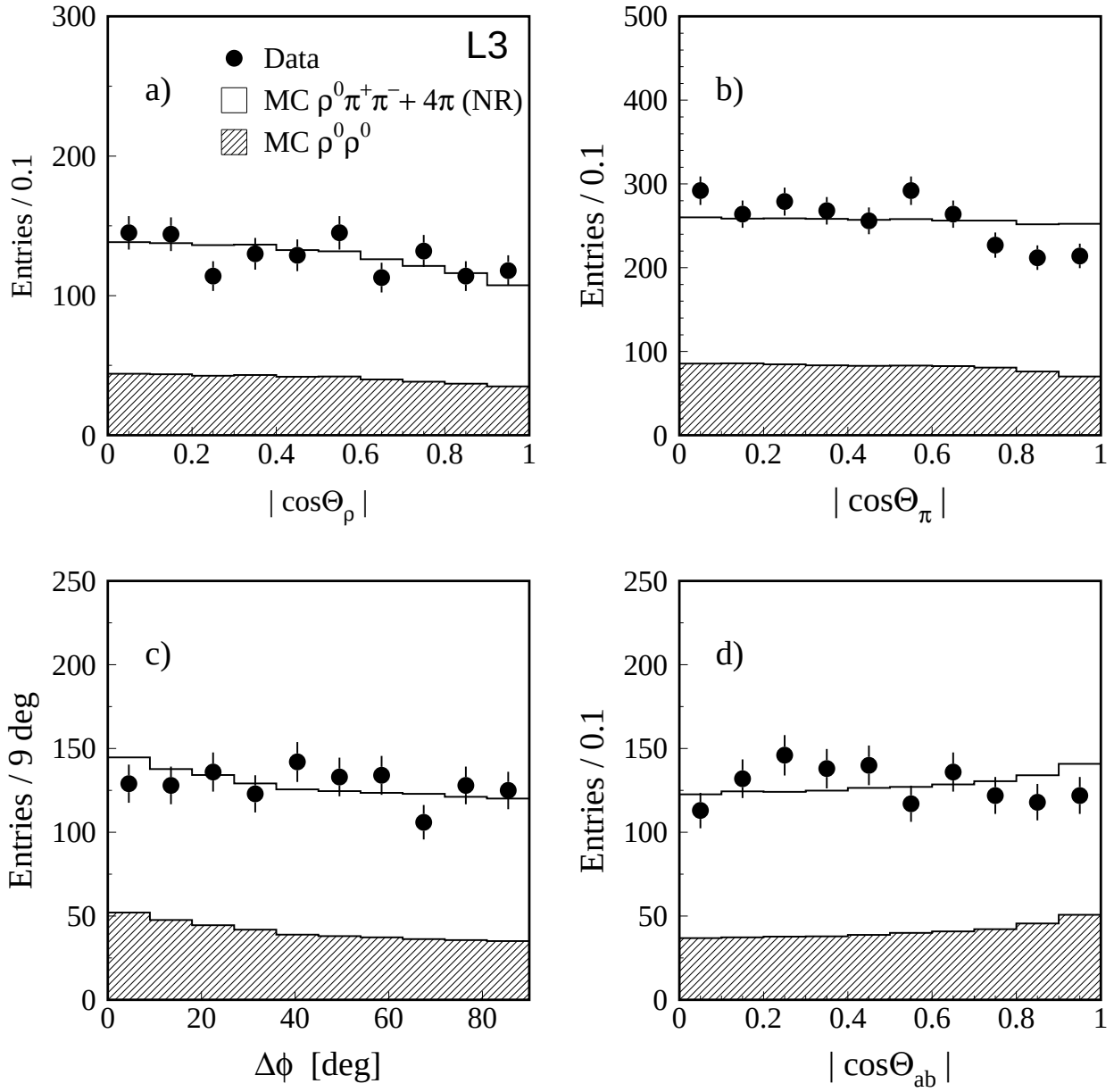

Figure 4: Comparison of data and Monte Carlo angular distributions: (a) $|\cos\theta_\rho|$, the cosine of the polar angle of the ρ^0 with respect to the $\gamma\gamma$ axis in the $\gamma\gamma$ center-of-mass system; (b) $|\cos\theta_\pi|$, the cosine of the polar angle of the pion in its parent ρ^0 helicity-system; (c) $\Delta\phi$, the angle between the decay planes of the two ρ^0 mesons in the $\gamma\gamma$ centre-of-mass system; (d) $|\cos\theta_{\rm ab}|$, the cosine of the opening angle between the two π^+ directions of flight, each one defined in its parent ρ^0 rest-system. There are two entries per event in (a),(c) and (d) and four entries per event in (b). The points represent the data, the hatched area shows the $\rho^0\rho^0$ component and the open area shows the sum of $\rho^0\pi^+\pi^-$ and $\pi^+\pi^-\pi^+\pi^-$ (non-resonant) components. The fraction of the different components are determined by the fit and the total normalisation is to the number of the events.

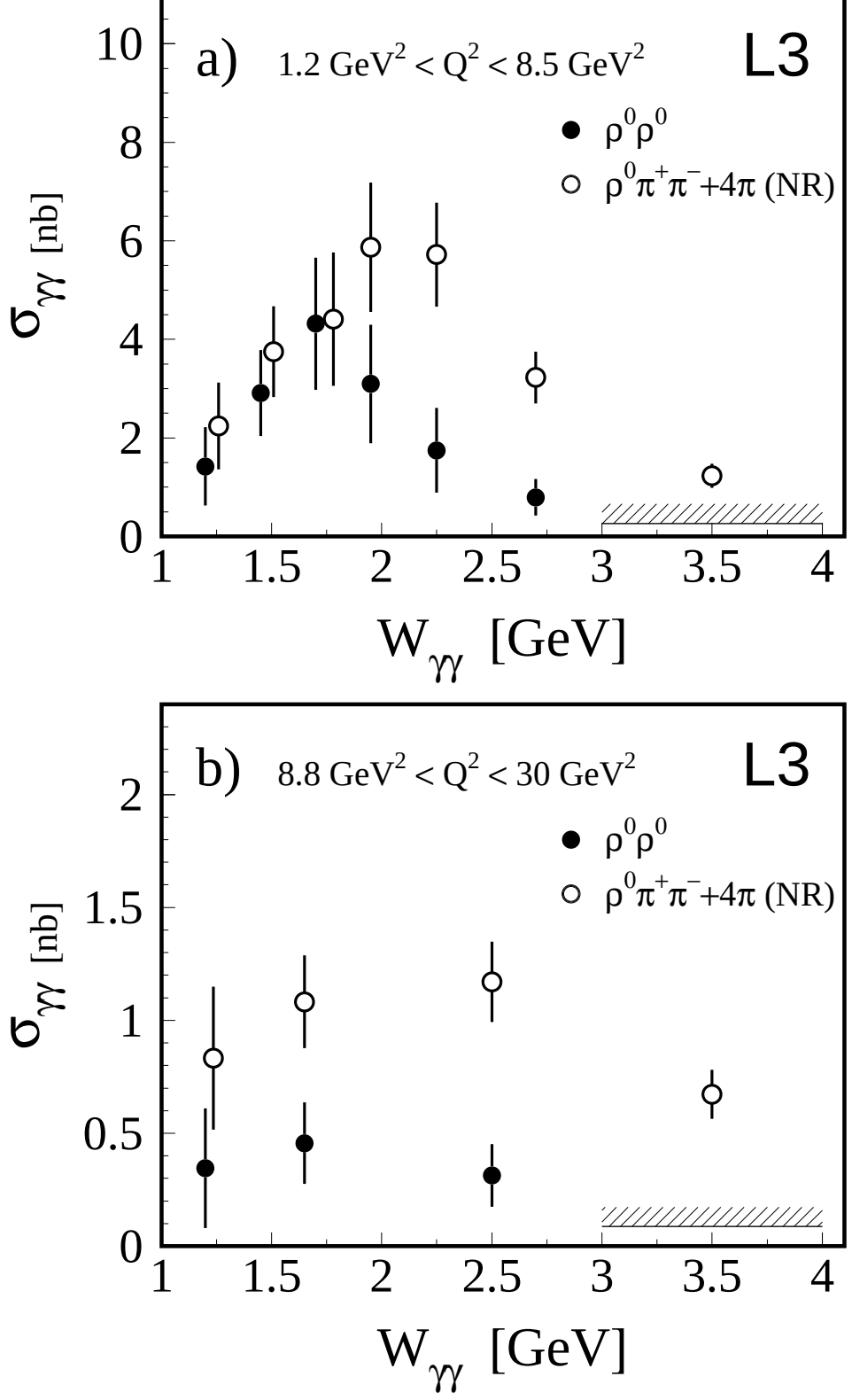

Figure 5: Cross section of the process $\gamma\gamma^* \to \rho^0\rho^0$ and the sum of the cross sections of the processes $\gamma\gamma^* \to \rho^0\pi^+\pi^-$ and $\gamma\gamma^* \to \pi^+\pi^-\pi^+\pi^-$(non-resonant) as functions of $W_{\gamma\gamma}$, for (a) 1.2 GeV^2 $< Q^2 <$ 8.5 GeV^2 and (b) 8.8 GeV^2 $< Q^2 <$ 30 GeV^2. The points represent the data, the bars show the statistical uncertainties. The horizontal line for the highest $W_{\gamma\gamma}$ bin indicates the upper limit of the $\gamma\gamma^* \to \rho^0\rho^0$ cross section at 95% CL: 0.26 nb for the Z-pole data and 0.087 nb for the high energy data.

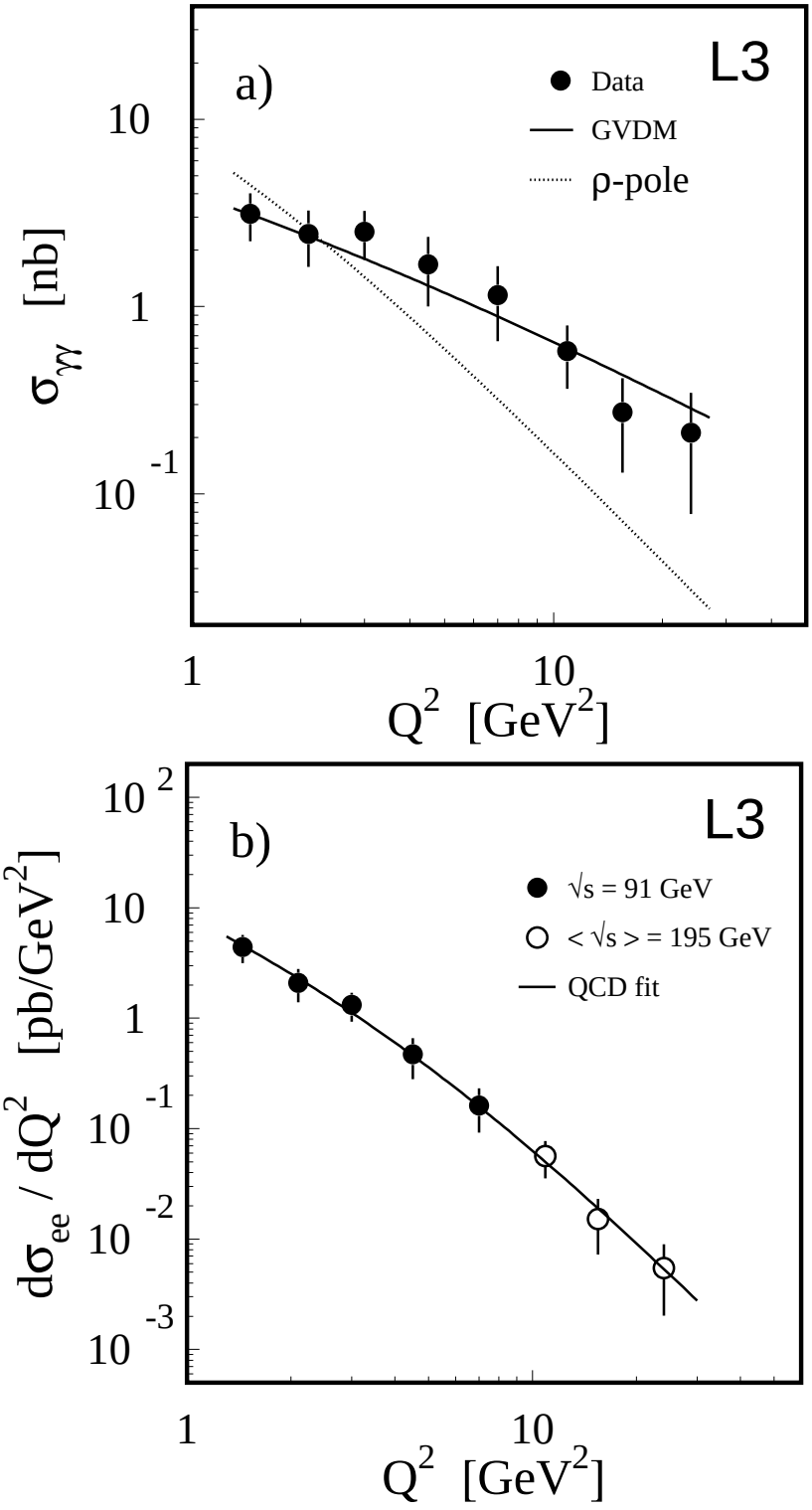

Figure 6: The $\rho^0\rho^0$ production cross section as a function of Q^2, for 1.1 GeV $< W_{\gamma\gamma} <$ 3 GeV: (a) cross section of the process $\gamma\gamma^* \to \rho^0\rho^0$ and (b) differential cross section of the process $e^+e^- \to e^+e^-\rho^0\rho^0$. The points represent the data, the bars show the statistical uncertainties. The solid line in (a) represents the result of a fit based on the generalized vector dominance model [6] and the dotted line indicates the expectation for a ρ-pole form-factor. The line in (b) represents the result of a fit to a form expected from QCD calculations.